Full length article

Establishing empirical relationships to predict porosity level and corrosion rate of atmospheric plasma-sprayed alumina coatings on AZ31B magnesium alloy

D. Thirumalaikumarasamy [a],*, K. Shanmugam [a], V. Balasubramanian [b]

[a] *Department of Manufacturing Engineering, Annamalai University, Annamalai Nagar 608 002, Chidambaram, Tamil Nadu, India*
[b] *Centre for Materials Joining and Research (CEMAJOR), Department of Manufacturing Engineering, Annamalai University, Annamalai Nagar 608 002, Tamil Nadu, India*

Abstract

Plasma sprayed ceramic coatings are successfully used in many industrial applications, where high wear and corrosion resistance with thermal insulation are required. In this work, empirical relationships were developed to predict the porosity and corrosion rate of alumina coatings by incorporating independently controllable atmospheric plasma spray operational parameters (input power, stand-off distance and powder feed rate) using response surface methodology (RSM). A central composite rotatable design with three factors and five levels was chosen to minimize the number of experimental conditions. Within the scope of the design space, the input power and the stand-off distance appeared to be the most significant two parameters affecting the responses among the three investigated process parameters. A linear regression relationship was also established between porosity and corrosion rate of the alumina coatings. Further, sensitivity analysis was carried out and compared with the relative impact of three process parameters on porosity level and corrosion rate to verify the measurement errors on the values of the uncertainty in estimated parameters.

* Corresponding author. Tel.: +91 9894319865 (mobile); fax: +91 4144 238080, +91 4144 238275.

E-mail addresses: tkumarasamy412@gmail.com, kumarthirumalai68@ymail.com (D. Thirumalaikumarasamy), drshanmugam67@gmail.com (K. Shanmugam), visvabalu@yahoo.com, balasubramanian.v.2784@annamalaiuniversity.ac.edu (V. Balasubramanian).

Production and hosting by Elsevier

1. Introduction

Magnesium alloys, which are one of the lightest engineering materials, have attracted much attention as promising materials for manufacturing structural parts such as the aerospace, automobile, and railway industries [1−3] because they can contribute to suppress fuel consumption and reduce CO_2 emission due to a reduction in weight of materials. However, the poor corrosion resistance of the magnesium alloys intensely limits their application. The poor corrosion resistance of the magnesium alloys is due to that they are relatively reactive and tend to suffer severe corrosion [4]. Various methods such as cathodic protection, corrosion inhibitor technique and covering the magnesium alloys with coatings or

Nomenclature

APS	atmospheric plasma spraying process
P	power, kW
S	stand-off distance, cm
F	powder feed rate, gpm
PL	porosity level, vol%.
CR	corrosion rate, mm/y
RSM	response surface methodology

films are employed to protect the magnesium alloys against the corrosion. One of the most common routes to decrease the corrosion rate of magnesium is to deposit a protective coating onto the magnesium surface. The protective coating could be prepared by some kinds of techniques like microarc oxidation [5], anodizing [6] and physical vapour deposition [7]. Among the above mentioned various surface techniques, atmospheric plasma spraying is considered as an effective method to prevent corrosion of magnesium and its alloys [8].

APS is a versatile thermal spray process, however, melting of feed stock particles, flattening and solidification of plasma sprayed particles impinging on a substrate surface are very complex phenomena involving rapid changes in the dynamic and thermal state of the molten particles that depend on many factors [9]. It is difficult to setup the process control due to the involvement of many process parameters in APS during evolution of the complex microstructure of plasma-sprayed coating is related to a number of processing variables. The establishment of a rigorous relationship between spray parameters and structure of a coating is the key point which will lead to the production of a desirable coating. The mechanical properties of plasma-sprayed coatings are very strongly dependent on the microstructure, and this can be controlled by manipulating the plasma spray process parameters [10].

Plasma sprayed ceramic coating can protect magnesium alloys against the corrosion [11]. The ceramic coatings can work in environments where both wear and corrosion resistances are required, especially at an elevated temperature; other coatings, such as organic and metallic coatings, cannot compare [12]. Some of the applications of alumina are in bearings, valves, pump seals, plungers, engine components, rocket nozzles, shields for guided missiles, vacuum tube envelops, integrated circuits, etc [13].

Coating properties like porosity, Young's modulus, phase composition, and coating residual stresses determine to a large extent the performance of coating during service [14]. The porosity is usually used as a parameter of the structure of plasma sprayed coating [15]. The pores and cracks interfere with the direct flow of heat resulting in lower thermal conductivity. In aggressive environments, one of the major problems in using plasma-sprayed coatings is the presence of the open pores, closed pores and micro-cracks in the coatings [16]. Moreover, the presence of even insignificant micropores can substantially reduce the coating's mechanical and protective properties, such as elastic modulus, micro-hardness and

bonding strength, etc. Therefore, reduction of porosity of the sprayed coatings plays a key role in improving the corrosion resistance of the coatings.

Many studies have contributed to a better understanding of the metallographic preparation, microstructure, thermal conductivity and diffusivity, residual stresses, and failure mechanisms of the ceramic coatings [17]. The impacts of the plasma spray process parameters on the coating characteristics and properties have generally been studied by means of classical one-factor-at-a-time or empirical approaches. Plasma spraying, however, involves many parameters and complex interactions among them. The one-factor at-a-time approach requires prohibitively large numbers of trials to systematically identify the effects of the process parameters, and therefore the effects of the process parameters on the microstructure and properties of the ceramic coatings have not been fully understood yet. Statistical designs of experiments have been shown to provide efficient approaches to systematically investigate the process parameters of thermal spray.

Researchers across the globe, tried to model thermal spraying processes using statistical regression techniques. Mawdsley et al. [18] reported that the statistically designed experiments and multiple regression analysis to identify the effects of process parameters on three properties of plasma sprayed alumina coatings, namely permeability, hardness and thickness. The Taguchi method was efficiently used by Kingswell et al. [19] to investigate the vacuum plasma spray deposition of alumina, nickel-based alloys, and tungsten carbide/cobalt cermet coatings. The small central composite design method was employed by Wang and Coyle [20] to optimize solution precursor plasma spray process parameters to deposit NiYSZ coatings on SOFCs. Statistical design of experiment by the response surface methodology (RSM) was used to successfully optimize the microhardness of plasma-sprayed WC-12%Co [21]. Li et al. [22] proposed models using uniform design method to analyse the dependence of deposition efficiency, porosity, oxide content, microhardness and fracture toughness on process parameters of plasma sprayed TiN coatings. Again, Li et al. [23] used a uniform design of experiments for optimizing the plasma spray process parameters of yttria stabilized zirconia coatings. The results of their investigation showed that the third-order regression equations were the most appropriate ones to identify the influence of process parameters. Azarmi et al. [24] et al. developed aD-optimal experimental design to characterize the effects of atmospheric plasma spray process parameters on in-flight particle temperature and velocity, and on the oxide content and porosity in a nickel based super-alloy coating. Lin et al. [25] adopted the design of orthogonal arrays for the seven three-level factors and the other two-level factor to optimize plasma spray parameters for the response of Vicker's hardness in a partially stabilized yttria stabilized zirconia coatings.

Though extensive research has been performed to model this process, the reported research work on relating the process parameters and coating characteristics is very scanty. Moreover, no systematic study has been reported so far to correlate the process parameters with porosity and corrosion rate.

Hence, in this work, an attempt was made to develop empirical relationship to predict the porosity and corrosion rate of plasma sprayed alumina coatings on AZ31B magnesium alloy using statistical tools such as design of experiments, analyses of variance and regression.

2. Methodology

2.1. Identifying the important process parameters

From the literature [18−25] and the preliminary work under taken [26], the predominant factors (APS process parameters) that have a greater influence on the coating properties were identified. They are (i) the power (kW), (ii) the stand-off distance (cm), (iii) the powder feed rate (gpm). These are the primary operational parameters contributing to the melting and flattening of the powder particles, subsequently, influencing the coating characteristics of plasma sprayed coatings.

2.2. Finding the working limits of the parameters

The chemical compositions of the AZ31B alloy used in this study are as follows: Mg-3.0Al−0.1Zn−0.2Mn (wt-%). The cut sectional surface of AZ31B magnesium alloy rod (16 mm in diameter and 15 mm in thickness) was grit blasted using cabinet type grit blasting machine prior to plasma spraying. Grit blasting was carried out using corundum grits of size of 500 + 320 μm and subsequently cleaned using acetone in an ultrasonic bath and dried. A large number of spraying trials

were conducted on grit blasted extruded AZ31B magnesium alloy to determine the feasible working limits of plasma spraying parameters. Plasma spraying of the alumina powder was carried out using an APS system 40 kW insulated gate bipolar transistor based Plasmatron (Make: Ion Arc Technologies; India. Model: APSS-II). The feed stock was H.C. Stark, AMPERIT 740.1 powder (Al_2O_3) with particle size of −45 + 20 μm. Coating thickness for all the deposits was maintained at 200 ± 15 μm. This was achieved using the following method. The values of the factors were set in the machine as prescribed by a run in the design matrix, after which one single layer was made. The gun traverse rate was constant for all experiments; it was 300 mm s^{-1}, and the coating track overlap was 30%. The thickness of the single layer made after the run was measured using a digital micrometer (model DIGIMATIC MDC-25SB). The number of passes required to achieve 200 μm thickness was determined, and the spray run was carried out to achieve it.

The input power, stand-off distance and powder feed rate were examined to identify the feasible working limits of the plasma spraying parameters, leading to the following observations and also seen in Table 1.

(1) If the spray was carried out below 18 kW power level, then poor adhesion and incomplete melting of powders were occurred. If the power level was increased beyond 25 kW, overheating of the substrate, formation of cracks and splashing were noticed during spraying.
(2) If the stand-off distance was less than 10 cm, then the arc length was short and also substrate deformation with

Table 1
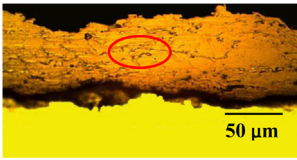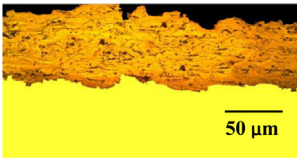Microstructure observation for fixing the working range of parameters.

Parameters	Parameter range	Microstructure	Name of the defect
Power	<18 kW	50 μm	Poor melting, unmelted particles present in the coating matrix
Power	>25 kW	50 μm	Vapour entrapment in the deposit and poor deposition efficiency
Stand-off distance	<10 cm	50 μm	Coating delamination
Stand-off distance	>13 cm	50 μm	Resoldification of molten particles and more interfacial cracks

Table 2
Important factors and their levels.

Factors	Notations	Units	Levels				
			−1.682	−1	0	+1	1.682
Power	P	kW	18	19.4	21.5	23.6	25
Stand-off distance	S	Cm	10	10.6	11.5	12.4	13
Powder feed rate	F	Gpm	15	20	25	30	35

delamination was observed. Stand-off distance greater than 130 mm resulted in an unstable arc and molten particles not reaching the target, this resulted in a poor deposition rate.

(3) The minimum possible powder feed rate was 15 gpm (limitation of the powder feeding system). If the powder feed rate was increased beyond 35 gpm, resulting in clogging of powder particles in the powder injection port.

2.3. Developing the experimental design matrix

Owing to a wide range of factors, the use of three-factor and five-level central composite rotatable design matrix was chosen to establish the empirical relationships for the responses using minimum possible number of experiments. Table 2 presents the ranges of factors considered, and Table 3 shows the 20 sets of coded conditions used to conduct the experiments. The method of designing such a matrix is dealt with elsewhere [27]. For the convenience of recording and processing experimental data, the upper and lower levels of the factors are coded here as +1.682 and −1.682 respectively. The coded values of any intermediate value can be calculated using the following relationship

$$X_i = 1.682[2X − (X_{max} + X_{min})]/(X_{max} − X_{min}) \quad (1)$$

Where,

X_i is the required coded value of a variable X and X is any value of the variable from X_{min} to X_{max};
X_{min} is the lower level of the variable;
X_{max} is the upper level of the variable.

2.4. Recording responses

In this present investigation, the plasma spraying was carried out according to the design of experiments, at each condition, three specimens were coated as prescribed by the design matrix. The experiments were conducted in a random order to prevent systematic errors infiltrating the system.

2.4.1. Porosity analysis

The porosity was analysed as per ASTM B276 standard [28] on the polished cross-section of the coating using optical microscope (Model: Meiji MIL-7100) equipped with image analysing system. Customary metallographic procedures were adopted to polish the cross-section of the coatings. A 200 μm square area was selected on the polished cross-section of the coating, and the image was analysed (Fig. 1). The same procedure was repeated at five random locations to find out the average percentage volume of porosity.

The steps involved in image analysis are shown in Table 4 and results shows the presence type A and type B pores usually formed in plasma sprayed coatings. Pore size and pores classified from 0 to 10 μm as type A and designated as A02, A04, A06 and A08. Pores Classification in the range from 10

Table 3
Design matrix and experimental results.

| Expt number	Coded values			Original value			Porosity level (vol. %)	Corrosion rate (mm/year)
	P	S	F	P (kW)	S (cm)	F (gpm)		
1	−1	−1	−1	19.4	10.6	20	12	15.92
2	1	−1	−1	23.6	10.6	20	7	7.92
3	−1	1	−1	19.4	12.4	20	14	14.35
4	1	1	−1	23.6	12.4	20	6	9.92
5	−1	−1	1	19.4	10.6	30	10	11.23
6	1	−1	1	23.6	10.6	30	9	8.90
7	−1	1	1	19.4	12.4	30	18	15.80
8	1	1	1	23.6	12.4	30	13	15.56
9	−1.682	0	0	18	11.5	25	14	19.02
10	1.682	0	0	25	11.5	25	5	12.98
11	0	−1.682	0	21.5	10	25	9	9.80
12	0	1.682	0	21.5	13	25	15	15.34
13	0	0	−1.682	21.5	11.5	15	8	6.12
14	0	0	1.682	21.5	11.5	35	12	6.89
15	0	0	0	21.5	11.5	25	5	5.02
16	0	0	0	21.5	11.5	25	6	4.98
17	0	0	0	21.5	11.5	25	5	5.53
18	0	0	0	21.5	11.5	25	6	4.89
19	0	0	0	21.5	11.5	25	5	5.92
20	0	0	0	21.5	11.5	25	5	4.99
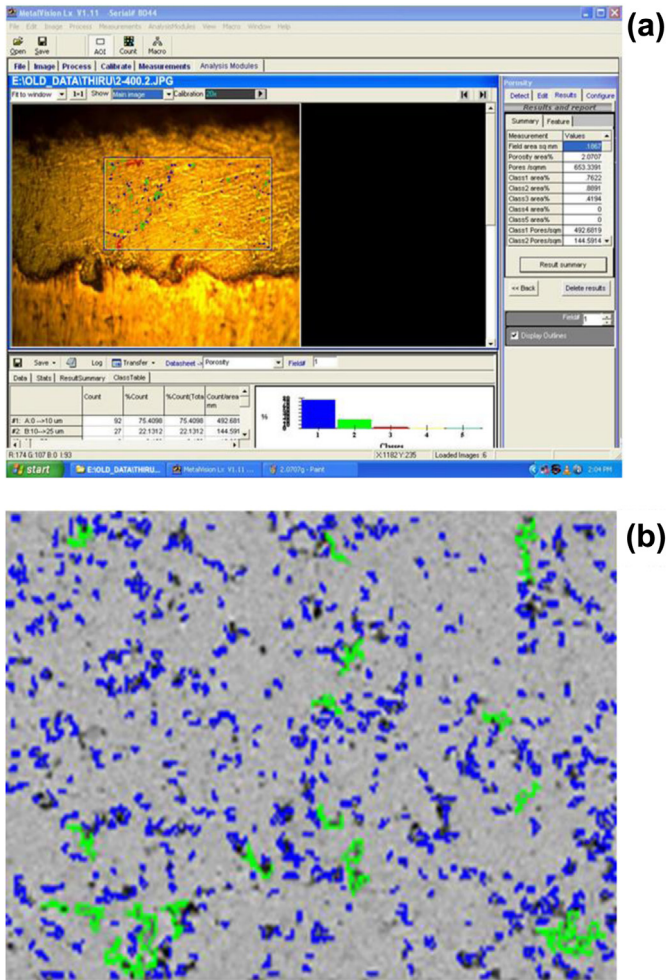
Fig. 1. Steps involved in coating porosity analysis and results of coating porosity analysis for Expt. no.6. (a) Optical image selected for analysis, Expt. No. 6, (b) colour coded overlay image for pore identification.

to 25 μm as type B and designated as B02, B04, B06 and B08. Type A pores may be formed as a result of interaction between material particles and the gaseous media. The type B pores are caused by the splashing of particles on impact with deposited material; or it may be due to voids resulting from the poor deformation of partially melted particles. These pores can have different sizes and exceedingly intricate shapes [29].

Table 4
Results summary of porosity analysis.

Total area measured			0.0432 sq.mm
Porosity	8.6%	Pores/sq.mm	2796.8
classes	Area %	Pores/sq.mm	Type
0 > 10 μm	1.8	2098.69	A08
10 > 25 μm	3.9	642.52	B08
25 > 75 μm	3.5	49.87	—
75 > 125 μm	0	0	—
>125 μm	0	0	—

Moreover, the results show that coating consists of type A and type B pores and distributed as A08 and B08 form which is evidence of the characteristics of plasma sprayed coating.

2.4.2. Corrosion testing

The corrosion behaviour of the coatings were evaluated by conducting immersion corrosion test in a 3.5% NaCl solution with a constant pH value of 7 and exposure time of 6 h. Fig. 2 presents the details of corrosion test. The specimens were ground with 500#, 800#, 1200#, 1500# grit SiC paper washed with distilled water and dried by warm flowing air. The corrosion rates of the as coated specimens were estimated through the weight loss measurement. The original weight (W_O) of the specimen were recorded and then immersed in the solution of 3.5% NaCl solution for 6 h. Finally, the corrosion products were removed by immersing the specimens for one minute in the solution prepared by using 50 g chromium trioxide (CrO_3), 2.5 g silver nitrate ($AgNO_3$) and 5 g barium nitrate ($Ba(NO_3)_2$) for 250 ml distilled water. The final weight (wt) of the specimen was measured and the net weight loss was calculated using the following equation [30]:

$$\text{Corrosion rate CR} = 87.6 \times W/A \times D \times T \qquad (2)$$

where W = weight loss in mg, A = surface area of the specimen in cm^2, D = density of the coated specimen, T = corrosion time in h.

The Scanning Electron Microscope (Make: Jeol, Japan; Model: 6410-LV) was used to analyse the size and morphology of the parent materials. The powder is fused and then crushed, which gives its characteristic angular shape as shown in Fig. 3. The X Ray Diffraction (Make: Rigaku, Japan; Model: ULTIMA-III) patterns of the powder and coating are shown in Figs. 4 and 5. The XRD pattern of the alumina powder exhibits α-Al_2O_3 phase only, whereas the XRD pattern of the sprayed coating shows α-Al_2O_3 as well as β-Al_2O_3 phases. Fig. 6(a) & (b) shows the optical microstructure and SEM images of the alumina coating. From these micro-graphs, it can be seen that the coating microstructure consists of completely melted splat structures, unmelted particulate regions, pores between the splats and cracks within the splats.

2.5. Theoretical approach

In this study, a response surface model building technique was utilised to predict porosity and corrosion rate in terms of various process parameters for APS process. The details of the model building technique are available in the literature [31,32].

### 2.5.1. Formulating empirical relationship

In the present investigation, to correlate the process parameters and the responses of APS coating deposits, a second order quadratic model was developed to predict the responses based on experimentally measured values. The responses are a function of power (P), stand-off distance (S), powder feed rate (F) and hence it can be expressed as
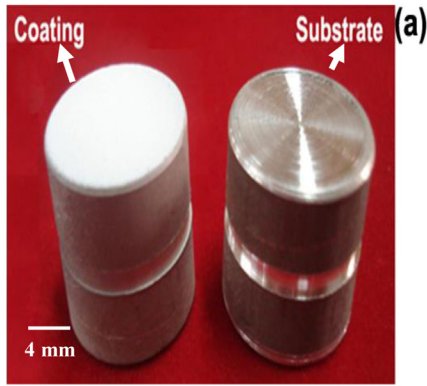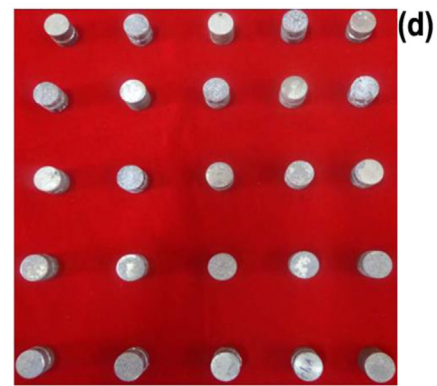
Photograph of uncoated and coated specimens (before corrosion test)
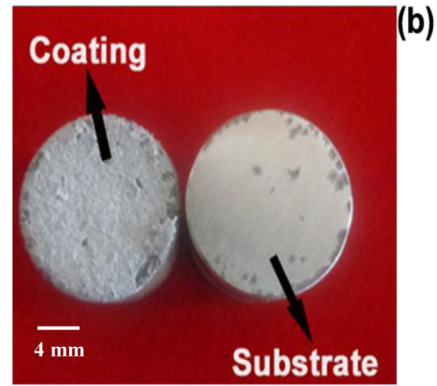
Photograph of uncoated and coated specimens (after corrosion test)
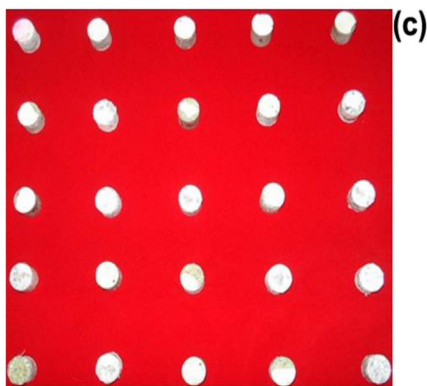
Photograph of uncoated specimens (after corrosion test)

Photograph of coated specimens (after corrosion test)

Fig. 2. Details of immersion corrosion test.

$$\text{Responses} = f(P, S, F) \tag{3}$$

The model chosen includes the effects of the main and interaction effects of all factors. The model selected is polynomial, and is expressed as follows:

$$Y = b_o + \sum b_i x_i + \sum b_{ii} x_i^2 + \sum b_{ij} x_i x_j \tag{4}$$

and for three factors, the selected polynomial could be expressed as

$$Y = b_0 + b_1(P) + b_2(S) + b_3(F) + b_{11}(P2) + b_{22}(S2) \\ + b_{33}(F2) + b_{12}(PS) + b_{13}(PF) + b_{23}(SF) \tag{5}$$
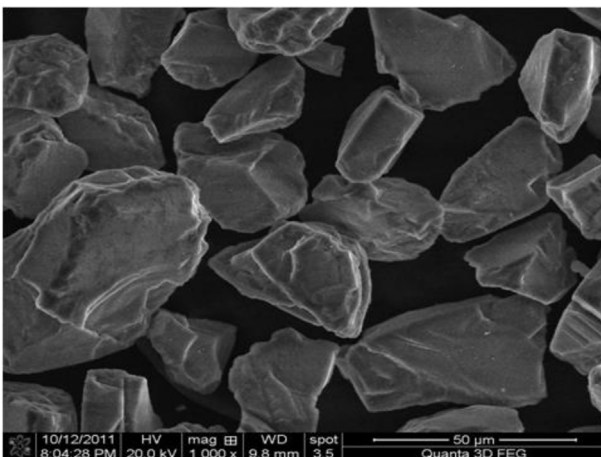

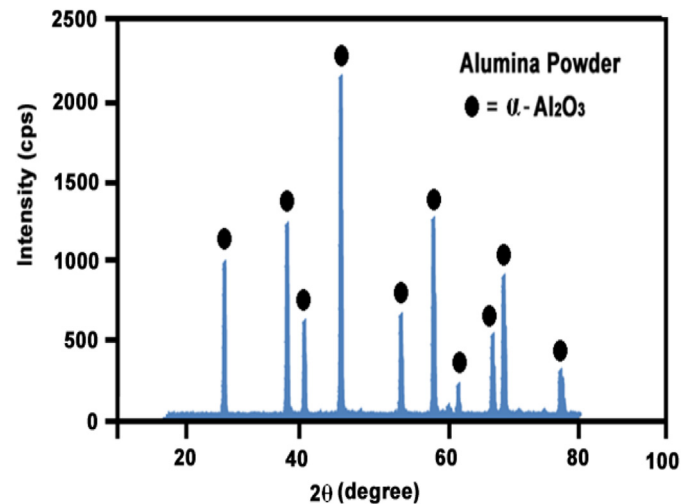Fig. 3. SEM micrograph of alumina powder.
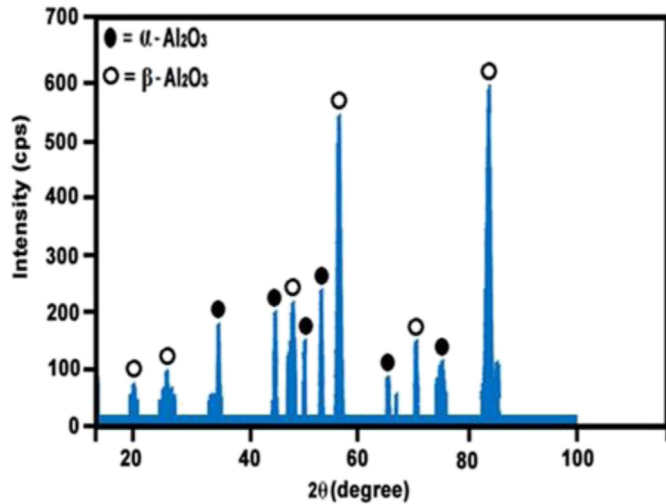

Fig. 4. XRD pattern of the alumina powder.

Fig. 5. XRD pattern of the alumina coating.

where b_0 is the average of the responses and b_1, b_2, b_3, …, b_{33} are regression coefficients that depend on respective linear, interaction, and squared terms of factors. In order to estimate the regression coefficients, a number of experimental design techniques are available. In this work, the central composite rotatable design was used which fits the second order response. All the coefficients were obtained applying central composite rotatable design using the Design Expert statistical software package (Version 8.07.1). The significance of each coefficient was determined by Student's *t* test and *p* values, which are listed in Tables 5 and 6. In this case, P, S, F, PS, PF, SF, P^2, S^2 and F^2 are significant model terms are shown in Tables 5 and 6, Values of "Prob>F" less than 0.05 indicate that model terms are significant. After determining the significant coefficients (at 95% confidence level), the final empirical relationship was constructed using only these coefficients and the final mathematical model to predict porosity and corrosion rate is given below:

$$
\begin{aligned}
\text{Porosity level (vol.\%)} = \ & 5.32 + 2.50(P) + 1.69(S) \\
& + 1.30(F)0.87(\text{PS}) + 0.88(\text{PF}) \\
& + 1.38(\text{SF}) + 1.54(\text{P2}) + 2.42(\text{S2}) \\
& + 1.72(\text{F2})
\end{aligned} \tag{6}
$$

$$
\begin{aligned}
\text{Corrosion rate (mm/year)} = \ & 5.22 - 1.84(P) + 1.54(S) \\
& + 0.34(F) + 0.71(PS) \\
& + 1.23(PF) + 1.35(SF) \\
& + 3.89(P2) + 2.67(S2) \\
& + 0.53(F2)\ \text{(mm/year)} \tag{7}
\end{aligned}
$$

2.5.2. Checking the adequacy of the model

In this investigation, analysis of variance (ANOVA) is used to check the adequacy of the developed empirical relationships [33]. ANOVA test results of the responses, namely, the porosity level and corrosion rate are presented in Tables 5 and 6, respectively. The adequacy of the model was tested using the ANOVA technique. In this study, the model *F* value and the associated probability values are checked to confirm the significance of the empirical relationships. Further, using the *F*-values, the predominant factors which have the major and minor effects on the responses could be assessed. From the *F* value assessment, it was found that the predominant factors which have direct influence on the responses as per hierarchy are power, stand-off distance and powder feed rate. The determination coefficient (R^2) indicates the goodness of fit for the model. In all the cases, the value of the determination coefficient ($R^2 > 0.99$) indicates that less than 1% of the total variations are not explained by the empirical relationships. The value of the adjusted determination coefficient is also high, which indicates the high significance of the empirical relationships. The predicted R^2 values also show good agreement with the adjusted R^2 values. Adequate precision compares the range of the predicted values at the design points with the average prediction error. At the same time, a relatively low value of the coefficient of variation indicates the improved precision and the reliability of the conducted experiments. The value of probability > *F* in Tables 5 and 6 for the empirical relationships are less than 0.05, which indicates that the empirical relationships are significant. Lack of fit was not significant for all the developed empirical relationships as desired [34]. The normal probability plots for the responses are shown in Fig. 7. From the figure, it could be inferred that the residuals fall on the straight line, which shows that the errors are distributed normally [35]. Collectively, these results
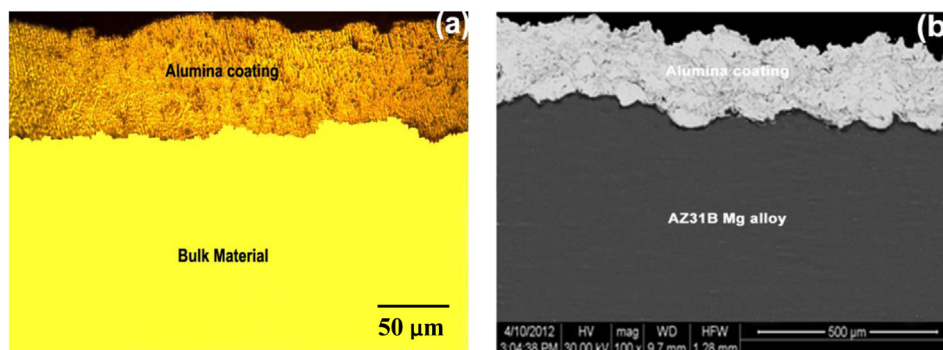

Fig. 6. Optical microstructure and SEM image of alumina coating.

Table 5
ANOVA test results for porosity level.

Source	Sum of squares	df	Mean square	F Value	p-value Prob > F	
Model	310.934	9	34.54822	152.4618	<0.0001	Significant
P	85.32534	1	85.32534	376.5419	<0.0001	
S	39.04143	1	39.04143	172.2903	<0.0001	
F	23.01061	1	23.01061	101.5462	<0.0001	
PS	6.125	1	6.125	27.02971	0.0004	
PF	6.125	1	6.125	27.02971	0.0004	
SF	15.125	1	15.125	66.74683	<0.0001	
P^2	34.12865	1	34.12865	150.6102	<0.0001	
S^2	84.59198	1	84.59198	373.3056	<0.0001	
F^2	42.41991	1	42.41991	187.1996	<0.0001	
Residual	2.266025	10	0.226603			
Lack of Fit	0.932692	5	0.186538	0.699519	0.6477	Not significant
Pure Error	1.333333	5	0.266667			
Cor Total	313.2	19				
Std. Dev.	0.476028	R-Squared		0.992765		
Mean	9.2	Adj R-Squared		0.986253		
C.V. %	5.174216	Pred R-Squared		0.970673		
PRESS	9.185101	Adeq Precision		37.25676		

df: degrees of freedom; CV: coefficient of variation; F: Fisher ratio; p: probability.

indicate the excellent capability of the regression model. Further, correlation graphs were drawn relating experimental values and predicted values as shown in Fig. 8 and it is found that the developed empirical relationships can be effectively used for prediction purpose.

3. Results and discussion

3.1. Dependence of porosity and corrosion rate on spray parameters

The developed mathematical model can be used to predict the range of parameters used in the investigation by substituting their respective values in coded form. Based on these models, the main and interaction effects of process parameter on porosity level and corrosion rate were computed and plotted in graphical form as shown in Figs. 9 and 10.

From the figures, it can be inferred that at lower power levels gave improper melting of the particles, which resulted in poor quality coatings in terms of higher porosity and corrosion rate. At low spraying powers, the powder particles are poorly melted. When they impact on the substrate or the already formed coating, they are not able to spread out completely to form splats and therefore, could not conform to the surface [36]. In such a case, the interlamellar pores and cracks will be formed due to the solidification of the splats. Moreover, when the spraying power is relatively low, numerous unmelted and partially melted particles are existed in the coating. As the arc current increases, the total and the net available energies in the plasma increase. This condition

Table 6
ANOVA test results for corrosion rate.

Source	Sum of squares	df	Mean square	F Value	p-Value prob > F	
Model	404.847	9	44.983	249.2319	<0.0001	Significant
P	46.35474	1	46.35474	256.8322	<0.0001	
S	32.24242	1	32.24242	178.6417	<0.0001	
F	1.623079	1	1.623079	8.992797	0.0134	
PS	4.013228	1	4.013228	22.23561	0.0008	
PF	12.15097	1	12.15097	67.32342	<0.0001	
SF	14.56596	1	14.56596	80.70388	<0.0001	
P^2	217.629	1	217.629	1205.791	<0.0001	
S^2	103.0545	1	103.0545	570.9817	<0.0001	
F^2	4.056546	1	4.056546	22.47561	0.0008	
Residual	1.804865	10	0.180487			
Lack of Fit	0.961151	5	0.19223	1.139189	0.4449	Not significant
Pure Error	0.843715	5	0.168743			
Cor Total	406.6519	19				
Std. Dev.	0.424837	R-Squared		0.995562		
Mean	10.05754	Adj R-Squared		0.991567		
C.V. %	4.224065	Pred R-Squared		0.978082		
PRESS	8.912924	Adeq Precision		46.90273		

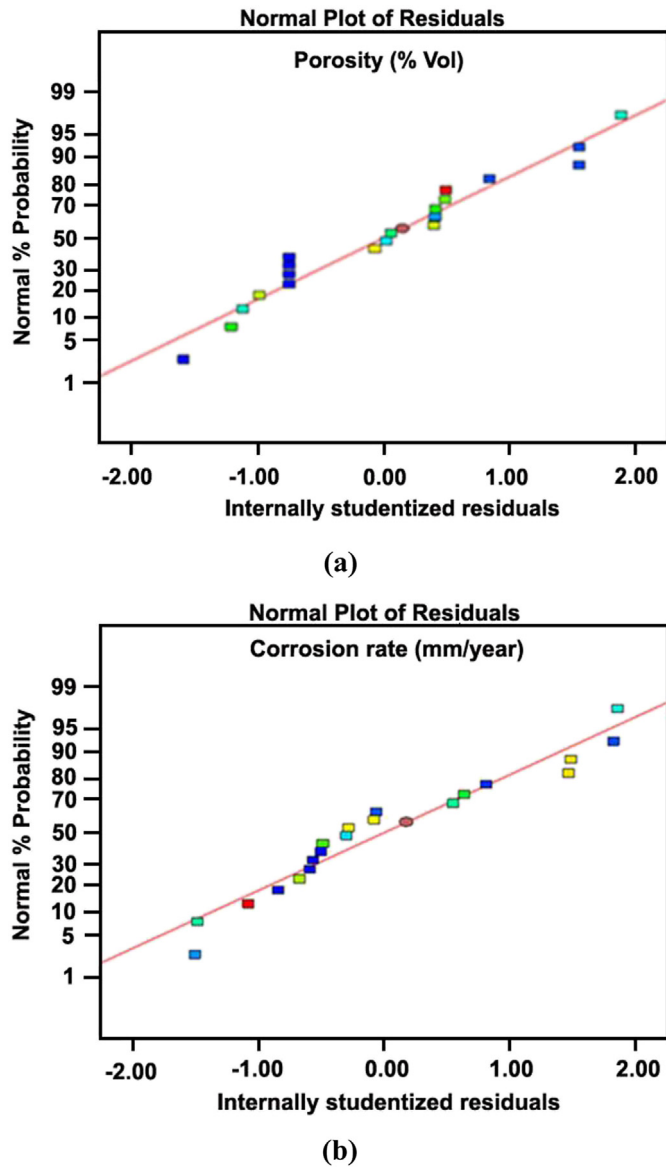df: degrees of freedom; CV: coefficient of variation; F: Fisher ratio; p: probability.

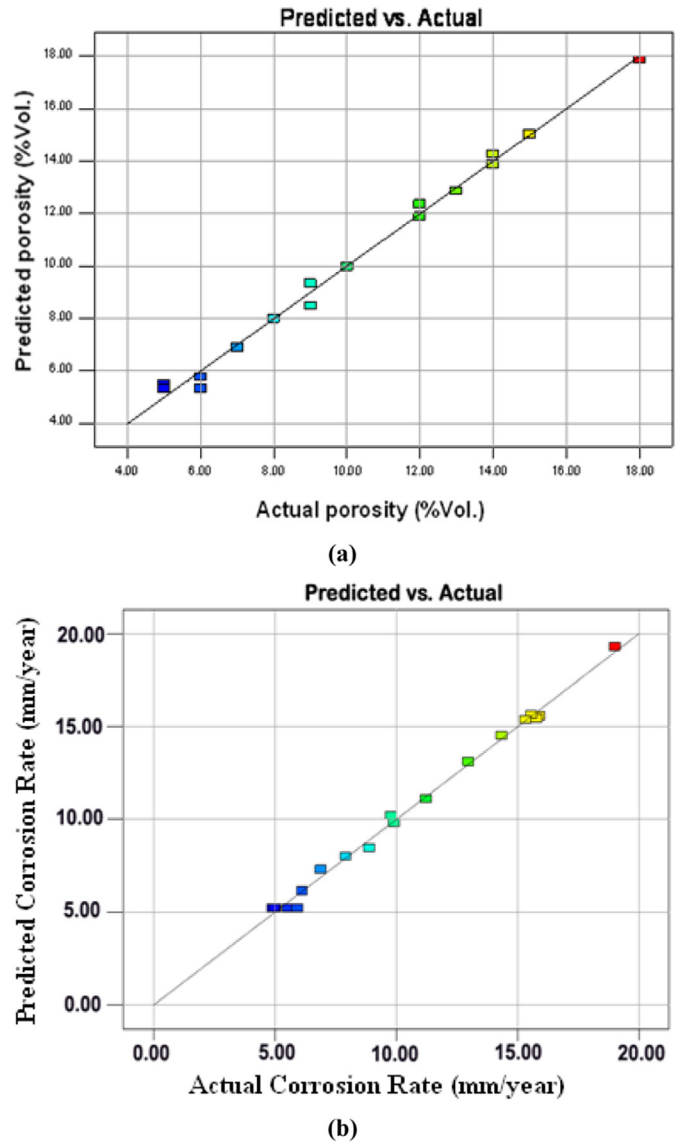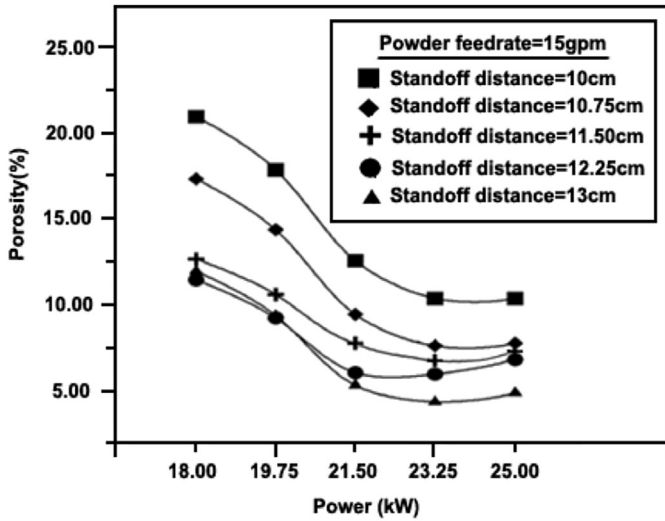Fig. 7. Normal probability plots for the responses.

Fig. 8. Correlation plots for the responses.

leads to a better in-flight particle molten state and higher velocities. It is well known that during plasma spraying, an electric arc is initiated between the two electrodes using a high frequency discharge and then sustained using power. The arc ionizes the gas, creating high-pressure gas plasma contains higher heat content. The resulting increase in gas temperature, which may exceed 30,000 °C, in turn increases the volume of the gas. The coatings are formed by spreading of melted droplets. Complete melting of the powders and higher velocity will yield lesser porosity coatings and make the melted droplets spread adequately. Increasing the power level increases the enthalpy in the plasma flame is likely to melt the particles, which in turn increases particle-melting ratio subsequently enhances good compaction of the coating obtained during the coating buildup. Further, effective flattening and solidification of the particles over the deposited layers will lead to reduce the porosity [37,38] and corrosion rate values.

Both the experimental and the predicted results agree in describing these effects.

The stand-off distance mainly controls the cohesion between splats because the temperature and velocity of particles in the plasma flame significantly change with stand-off distance. Therefore, better spreading and cohesion would be achieved with shorter spraying distances [39]. At smaller stand-off distance, possibility of splashing of molten particles and quench cracks end up with increased level of porosity [40]. Stand-off distance is of substantial importance because adequate distance must be provided for heating and accelerating the powder, but too great a distance will allow the powder to cool and lose velocity, because the gas stream is rapidly expanding, cooling, and slowing will end up with molten droplets land on substrate without enough kinetic energy to form splats. These droplets can stay on the substrate by themselves [41] and acts as a stress concentrator which resulted in crack propagation in multiple directions. With

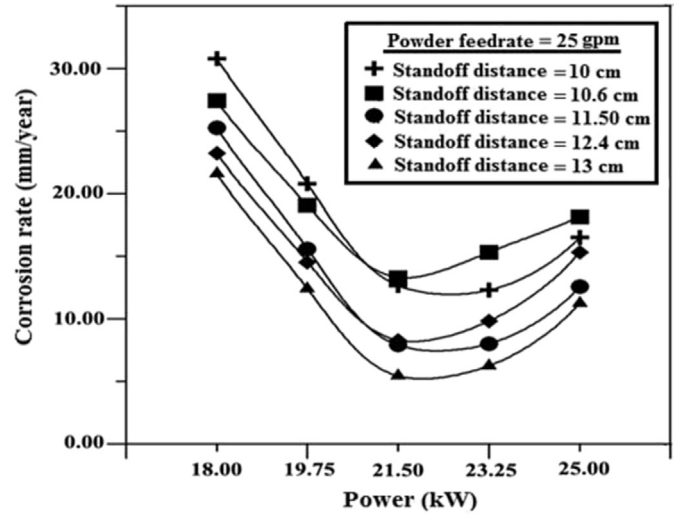Effect of power and standoff distance on porosity

Effect of power and stand-off distance on corrosion rate
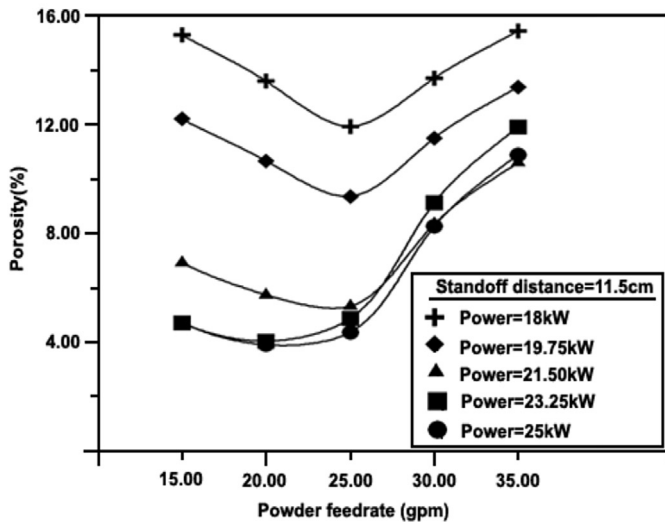
Effect of powder feed rate and power on porosity

Fig. 9. Effect of plasma spray parameters on porosity.

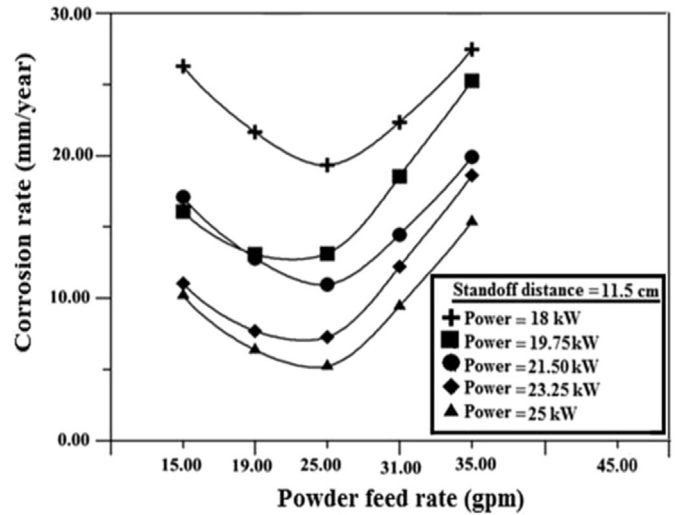Effect of powder feed rate and power on corrosion rate

Fig. 10. Effect of plasma spray parameters on corrosion rate.

longer stand-off distances, the enthalpy of the molten ceramic particles is largely lost, and the particles are decelerated in a relatively longer flight path because of the interaction with the surrounding air. Under such conditions, the particles striking on the substrate will not be adequately flattened to overlap the layers, resulting in increasing porosity, and corrosion rate values (Figs. 9 and 10).

The variations in the powder feed rate on the responses are displayed in Figs. 9 and 10. Too low a powder feed rate will result in vaporization, and over melting of the particles resulting in quench cracks [42,43], splashing, and high porosity levels, whereas too high a feed rate will end up in poor melting of the powder particles resulting in a decrease of the splat flattening ratio and an increase in the porosity. At high powder feedrate, the heat content in the plasma gas becomes insufficient for the melting of the powder particles. The poorly melted (unmelted and partially melted) particles will be remained in the coating, resulting in a less dense coating with high porosity and corrosion rate. This result indicates that when the powder feedrate is high, the particles which obtain low thermal energy and kinetic energy cannot be fully melted. Considering individual process parameter, the porosity and corrosion rate was less sensitive to the powder feed rate which has good agreement with 'F' value in Tables 4 and 5.

3.2. Relationship between porosity and corrosion rate of alumina coatings

The coating porosity and the corrosion rate obtained from the experimental results are related as shown in Fig. 11. The experimental data points are fitted by a straight line. The straight line is governed by the following regression equation:

$$\text{Corrosion rate (mm/year)} = 1.721 + 0.906(\text{porosity in vol.\%})$$
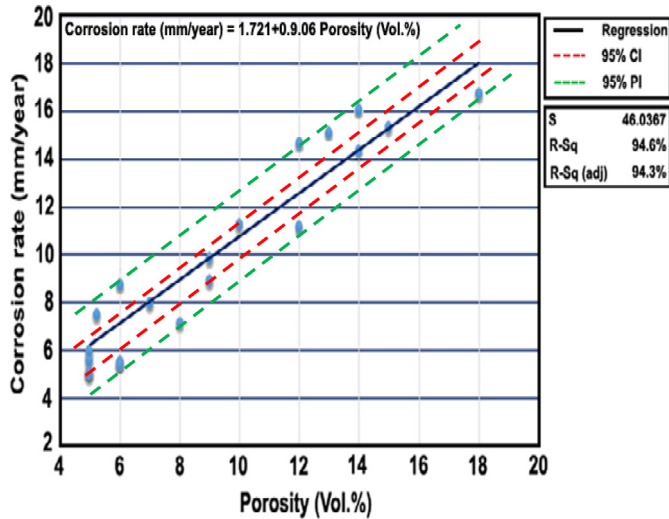
$$(8)$$

Fig. 11. Relationship graph for porosity and corrosion rate.

The slope of the estimated regression equation (+0.906) is positive, implying that as porosity increases, corrosion rate increases. The coefficient of determination is $R^2 = 94.6\%$. It can be interpreted as the percentage of the total sum of squares that can be explained by using the estimated regression equation. The coefficient of determination R^2 is a measure of the goodness of fit of the estimated regression equation [44].

The fitted regression line (Eq. (8)) may be used for two purposes:

(a) To estimate the mean value of corrosion rate for the given value of coating porosity.
(b) Predicting an individual value of corrosion rate for a given value of coating porosity level.

The confidence interval and prediction interval show the precision of the regression results. Narrower intervals provide a higher degree of precision (Fig. 11). Confidence interval (CI) is an interval estimate of the mean value of y for a given value of x. Prediction interval (PI) is an interval estimate of an individual value of y for a given value of x. The estimated regression equation provides a point estimate of the mean value of corrosion rate for a given value of porosity. The difference between CI and PI reflects the fact that it is possible to estimate the mean value of corrosion rate more precisely than an individual value of corrosion rate. The greater width of the PI is reflecting the added variability introduced by predicting a value of the random variable as opposed to estimating a mean value. From Fig. 11, it is also inferred that the closer the value to 'X' (15.21vol %) the narrower will be the interval.

4. Sensitivity analysis

Sensitivity analysis, a method to identify critical parameters and rank them by their order of importance, is paramount in model validation where attempts are made to compare the calculated output to the measured data. This type of analysis can be useful to find out, which input parameter must be most accurately measured, thus determining the input parameters exerting the most influence upon model outputs [45]. Therefore, sensitivity analysis plays an important role in determining which parameter of the process should be modified to obtain the improved response characteristics. Mathematically, sensitivity of a design objective function with respect to a design variable is the partial derivative of that function with respect to its variables. To obtain the sensitivity equation for input power, Eq. (11) with non significant terms is differentiated with respect to input power. The sensitivity Eqs. (9)−(11) represent the sensitivity of porosity level for input power, stand-off distance and powder feed rate, respectively.

$$\partial PL/\partial P = -2.50 - 0.87S + 0.88F + 3.08P \tag{9}$$

$$\partial PL/\partial S = 1.69 - 0.87P + 1.38F + 4.84S \tag{10}$$

$$\partial PL/\partial F = 1.30 + 0.88P - 1.38S + 3.44F \tag{11}$$

Similarly the sensitivity Eqs. (12)−(14) represent the sensitivity of corrosion rate for input power, stand-off distance and powder feed rate, respectively.

$$\partial CR/\partial P = -1.84 + 0.71S + 1.23F + 7.78P \tag{12}$$

$$\partial CR/\partial S = 1.54 + 0.71P + 1.35F + 5.34S \tag{13}$$

$$\partial CR/\partial F = 0.34 + 1.23P + 1.35S + 1.06F \tag{14}$$

In this study, the aim is to predict the tendency of responses due to a small change in process parameters for plasma spraying process. Sensitivity information should be interpreted using mathematical definition of derivatives. Namely, positive sensitivity values imply an increment in the objective function by a small change in design parameter whereas negative values state the opposite.

4.1. Evaluation of sensitivity results

Fig. 12 displays the input power, stand-off distance and powder feed rate sensitivity maps on porosity level respectively. From Fig. 12(a), it can be seen that the increase in porosity increases the positive sensitivity; the sensitivity is on the positive side. The largest positive variation was found at 18 kW, 13 cm and 35 gpm respectively. From Fig. 12(b), it can be observed that increase in stand-off distance increases the positive sensitivity. The maximum positive variation was found at 25 kW, 13 cm and 35 gpm. The largest negative variation was observed at 18 kW, 10 cm and 15 gpm. Fig. 12(c) indicates values less than 11.5 cm indicates negative values and greater than 11.5 cm shows positive sensitivity. The maximum positive variation was observed at 18 kW, 13 cm and 35 gpm. The largest negative variation was observed at 25 kW, 10 cm and 15 gpm.
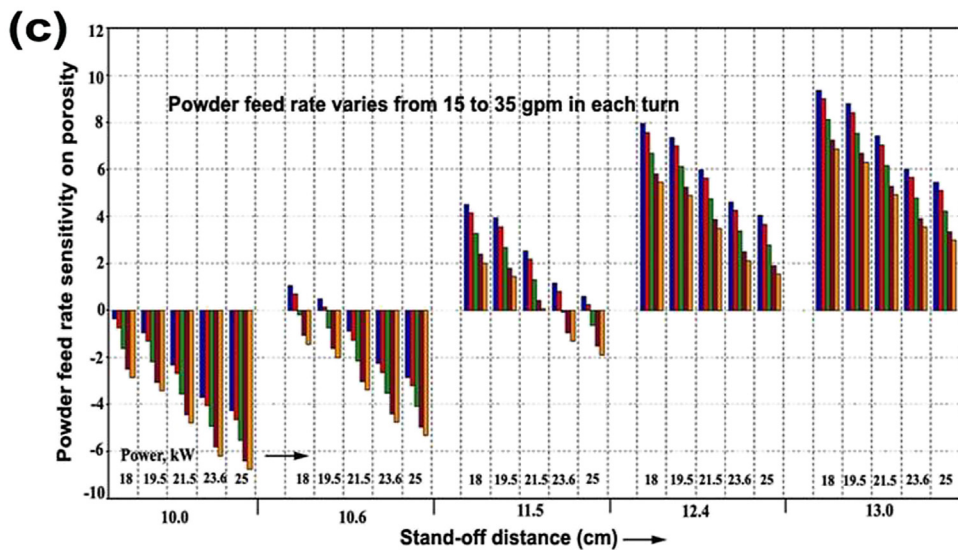
The input power, stand-off distance and powder feed rate sensitivity maps on corrosion rate is shown in Fig. 13. It is observed that the increase in corrosion rate, increases the
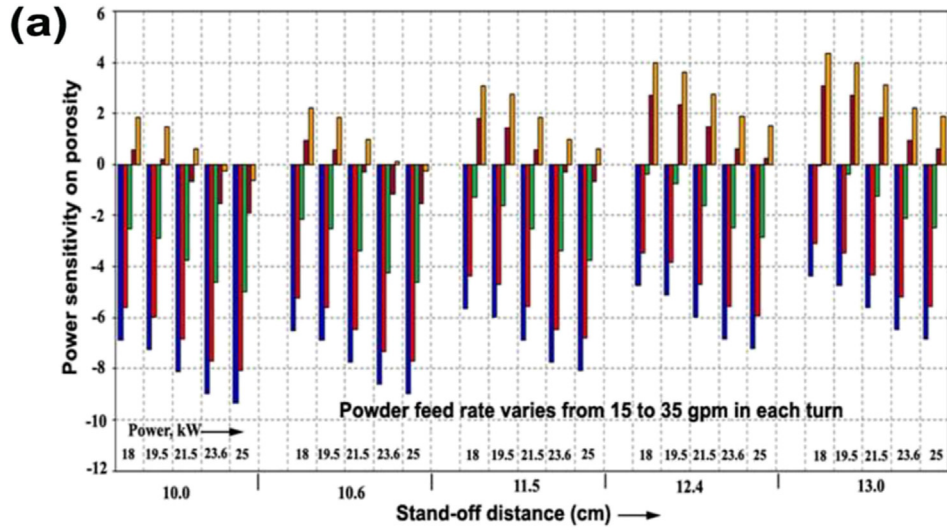
Sensitivity of input power on porosity level
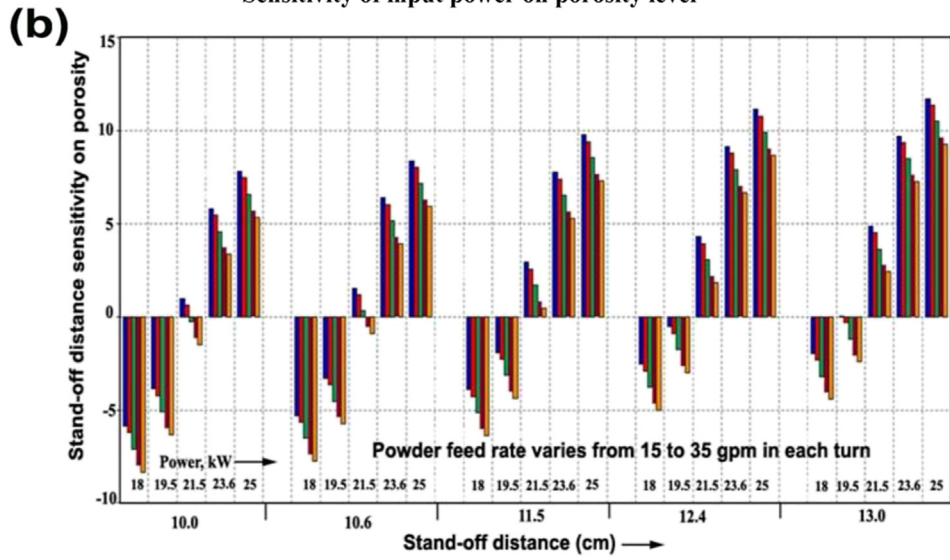
Sensitivity of stand-off distance on porosity level

Sensitivity of powder feed rate on porosity level

Fig. 12. Sensitivity analysis results for porosity level.

Sensitivity of input power on corrosion rate

Sensitivity of stand-off distance on corrosion rate

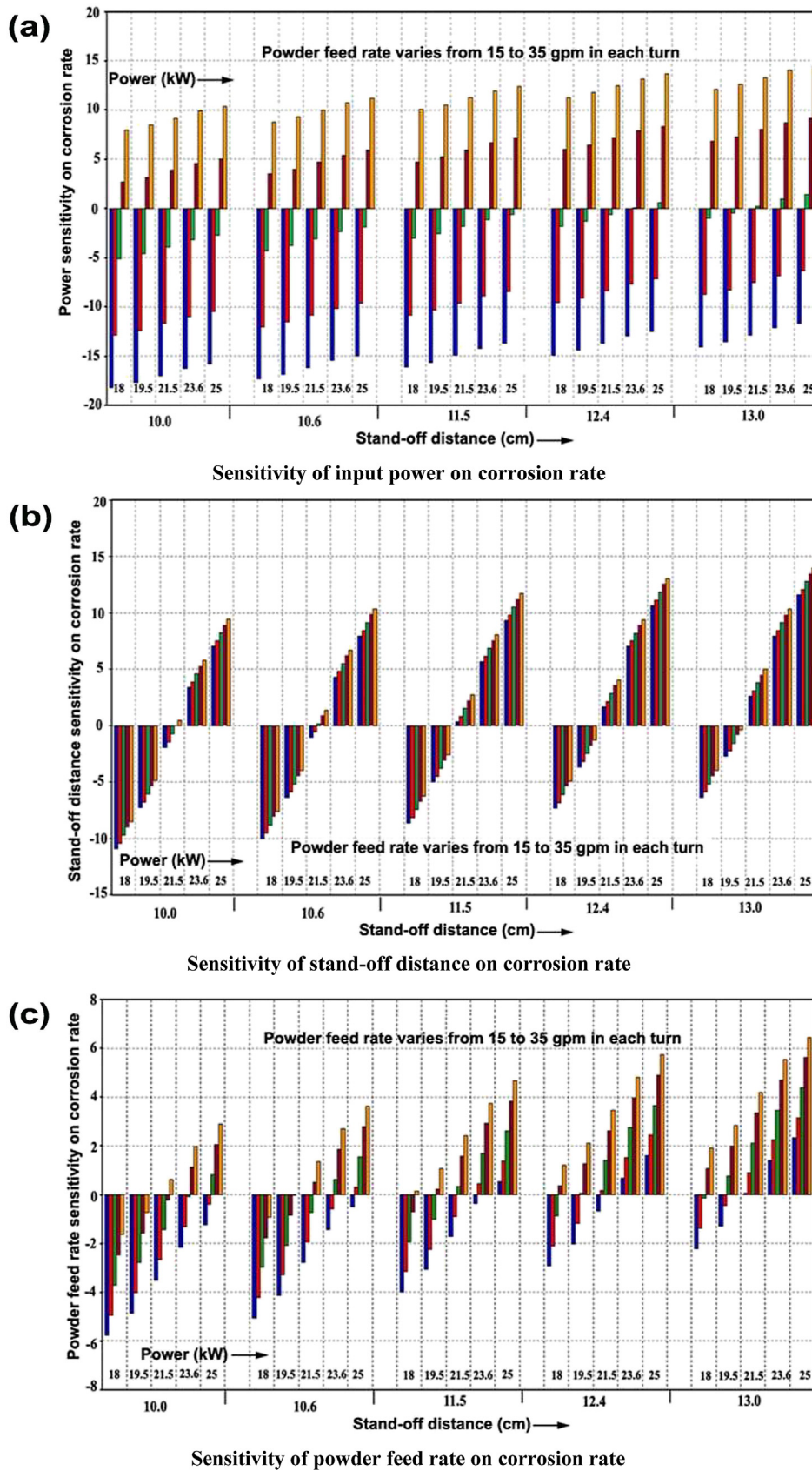**Sensitivity of powder feed rate on corrosion rate**

Fig. 13. Sensitivity analysis results for corrosion rate.

positive sensitivity; the sensitivity is on the positive side. The largest positive variation was found at 25 kW, 13 cm and 35 gpm respectively. From Fig. 13(b), it can be seen that increase in stand-off distance increases the positive sensitivity. The maximum positive variation was found at 25 kW, 13 cm and 35 gpm. The largest negative variation was observed at 18 kW, 10 cm and 15 gpm. Fig. 13(c) indicates values less than 11.5 cm indicates negative values and greater than 11.5 cm shows positive sensitivity. The maximum positive variation was observed at 25 kW, 13 cm and 35 gpm. The small variation of input power causes large changes in porosity level and corrosion rate (Figs.12 and 13). The results reveal that the porosity level and corrosion rate is more sensitive to input power than stand-off distance and powder feed rate.

5. Conclusions

1. Empirical relationships were developed to predict (at 95% confidence level) the porosity and corrosion rate of plasma sprayed alumina coatings on AZ31B magnesium alloy incorporating few important spray parameters, such as input power, stand-off distance and powder feed rate.
2. Input power has greater influence on porosity and corrosion rate, followed by stand-off distance and powder feed rate.
3. A regression equation has been developed incorporating porosity and corrosion rate of the plasma sprayed alumina coatings. This equation can be effectively used to predict plasma sprayed corrosion rate of alumina coating, if the coating porosity is known.
4. Input power was more sensitive than the other parameters such as stand-off distance and powder feed rate.

Acknowledgements

References

[1] J.E. Gray, B. Luan, J. Alloy. Compd. 336 (2002) 88.
[2] W.A. Ferrando, J. Mater. Eng. 11 (1989) 299.
[3] G.L. Song, Adv. Eng. Mater. 7 (2005) 563.
[4] J.E. Gray-Munro, B. Luan, L. Huntington, Appl. Surf. Sci. 254 (2008) 2871.
[5] X.G. Han, F. Zhu, X.P. Zhu, M.K. Lei, J.J. Xu, Surf. Coat. Technol. 228 (2013) 164.
[6] S. Verdier, M. Boinet, S. Maximovitch, F. Dalard, Corros. Sci. 47 (2005) 1429.
[7] M.H. Lee, Y.W. Kim, K.M. Lim, S.H. Lee, K.M. Moon, Trans. Nonferr. Met. Soc. China 23 (2013) 876.
[8] H. Singh, B.S. Sidhu, D. Puri, S. Prakash, Mater. Corros. 58 (2007) 92.
[9] P. Fauchais, M. Vardelle, A. Vardelle, L. Bianchi, Ceram. Int. 22 (1996) 295.
[10] D. Schwingel, R. Taylor, T. Haubold, J. Wigren, C. Gualco, Surf. Coat. Technol. 108 (1998) 99.
[11] D.R. Yan, J.N. He, J.J. Wu, W.Q. Qiu, J. Ma, Surf. Coat. Technol. 89 (1997) 191.
[12] Y. Wang, S. Jiang, M.D. Wang, S.H. Wang, T.D. Xiao, P.R. Strutt, Wear 237 (2000) 176.
[13] O. Sarikaya, Mater. Des. 26 (2005) 53.
[14] C.S. Ramachandran, V. Balasubramanian, P.V. Ananthapadmanabhan, Surf. Eng. 27 (2011) 217.
[15] C.J. Li, A. Ohmori, J. Therm. Spray. Technol. 11 (2002) 365.
[16] I.Y. Konyashin, T.V. Chukalovskaya, Surf. Coat. Technol. 88 (1996) 5.
[17] C.S. Ramachandran, V. Balasubramanian, P.V. Ananthapadmanabhan, J. Therm. Spray. Technol. 20 (2010) 590.
[18] J.R. Mawdsley, Y.J. Su, K.T. Faber, T.F. Bernecki, Mat. Sci. Eng. A 308 (2001) 189.
[19] R. Kingswell, K.T. Scott, L.L. Wassell, J. Therm. Spray. Technol. 2 (1993) 179.
[20] Y. Wang, T.W. Coyle, J. Therm. Spray. Technol. 17 (2008) 692.
[21] T. Troczynski, M. Plamondon, J. Therm. Spray. Technol. 1 (1992) 293.
[22] J.F. Li, H. Liao, B. Normand, C. Cordier, G. Maurin, J. Foct, C. Coddet, Surf. Coat. Technol. 176 (2003) 1.
[23] J.F. .Li, H.L. Liao, C.X. Ding, C. Coddet, J. Mat. Proc. Technol. 160 (2005) 34.
[24] F. Azarmi, T.W. Coyle, J. Mostaghimi, J. Therm. Spray. Technol. 17 (2008) 144.
[25] Bor-Tsuen Lin, Ming-Der Jean, Jyh-Horng Chou, Appl. Surf. Sci. 253 (2007) 3254.
[26] C.S. Ramachandran, V. Balasubramanian, P.V. Ananthapadmanabhan, V. Viswabaskaran, Mater. Des. 39 (2012) 234.
[27] R.G. Miller, J.E. Freund, D.E. Johnson, Probability and Statistics for Engineers, Prentice Hall of India Pvt Ltd., New Delhi, 1999, p. 75.
[28] ASTM B 276−05, Standard Test Method for Apparent Porosity in Cemented Carbides, American Society for Testing and Materials, Pennsylvania, 2010.
[29] Hao Du, Soo Wohn Lee, Jae Heyg Shin, J. Therm. Spray. Technol. 14 (2005) 453.
[30] ASTM G31-72, Standard Practice for Laboratory Immersion Corrosion Testing of Metals, 2002.
[31] K.Y. Benyounis, A.G. Olabi, Adv. Eng. Softw. 39 (2008) 483.
[32] A.R. Hamad, J.H. Abboud, F.M. Shuaeib, K.Y. Benyounis, Adv. Eng. Softw. 41 (2010) 674.
[33] H. Oktem, T. Erzurumlu, H. Kurtaran, J. Mater. Process. Technol. 170 (2005) 11.
[34] W.G. Cochran, G.M. Cox, Experimental Designs, second ed., John Wiley &Sons (Asia) Pte Ltd, Singapore, 1992.
[35] R.H. Myers, D.C. Montgomery, Response Surface Methodology, John Wiley &Sons, Inc., NewYork, 2002.
[36] O. Amsellem, F. Borit, D. Jeulin, V. Guipont, M. Jeandin, J. Therm. Spray. Technol. 21 (2012) 193.
[37] G. Montavon, C.C. Berndt, C. Coddet, S. Sampath, H. Herman, J. Therm. Spray. Technol. 6 (1997) 153.
[38] Dong Zhao, Fa Luo, Wancheng Zhou, Dongmei Zhu, Appl. Surf. Sci. 264 (2013) 545.
[39] J.G. La Barbera-Sosa, Y.Y. Santana, E. Moreno, N. Cuadrado, J. Caro, P.O. Renault, E. Le Bourhis, M.H. Staia, E.S. Puchi- Cabrera, Surf. Coat. Technol. 205 (2010) 1799.
[40] A. Kucuk, C.C. Berndt, U. Senturk, R.S. Lima, C.R.C. Lima, Mat. Sci. Eng. A 284 (2000) 29.
[41] S. Karthikeyan, V.Balasubramanian, R. Rajendran, Ceram. Int. 40 (2014) 3171.
[42] S. Kuroda, T. Fukushima, S. Kitahara, J. Therm. Spray. Technol. 1 (1992) 325.
[43] S. Kuroda, T. Dendo, S. Kitahara, J. Therm. Spray. Technol. 4 (1995) 75.
[44] S. Rajakumar, C. Muralidharan, V. Balasubramanian, Exp. Tech. 36 (2012) 6.
[45] A.S. Sarigu, A.A. Secgin, Appl. Acoust. 65 (2004) 1037.